Department of Clinical Laboratory, First Affiliated Hospital of Anhui Medical University, Hefei, China

Synthesis and antibacterial activity of novel icariin derivatives

A. Wang, Aili, Zhang, y. Xu*

Received November 9, 2018, accepted December 3, 2018

**Corresponding author: Yuanhong Xu, Department of Clinical Laboratory, First Affiliated Hospital of Anhui Medical University, Hefei 230032, China*
cym19841107@sina.com

Pharmazie 74: 73–78 (2019) *doi: 10.1691/ph.2019.8866*

A series of aromatic sulfonyls substituted icariin derivatives was synthesized and their antibacterial activities against *S. aureus* (including drug-sensitive bacteria and drug-resistant bacteria) were evaluated. Among them, compound **9** exhibited high potency against methicillin-sensitive (MSSA) and resistant strains of *S. aureus* (MRSA) with MIC values of 1-2 mmol/L. Reverse virtual screening and molecule docking analysis indicated that compound **9** might bind the allosteric site of PBP2a that may inhibit cell wall synthesis, with the advantage of activity against multidrug resistant *S. aureus.* SPR experiment further confirmed the binding affinity. Therefore, we consider aromatic sulfonyls at C-3 position substituted icariin derivatives to be a novel class of anti-MRSA agents worth of further investigation.

1. Introduction

The irrational usage of antibiotics and the bacterial drug resistance are two serious problems in the field of medical today, which to harm the life of people. The pandemic antibiotic-resistant infections caused by resistant Gram-positive bacteria such as methicillin-resistant *S. aureus* (MRSA) (Parrish et al. 2018) and *Staphylococcus epidermidis* (MRSE) (Lazaris et al. 2017), vancomycin resistant Enterococci (VRE) (MacAllister et al. 2018), and penicillin-resistant *Streptococcus pneumoniae* (PRSP) (Mamishi et al. 2018) are the main concern. Additionally, the current lack of sufficient and effective antimicrobial drugs and the scarce interest of pharmaceutical companies on developing novel antimicrobial drugs, point out that common bacterial infections might cause serious complications in a near future. Therefore, we need to develop new antibacterial drugs.

Flavonoids are widely found in many natural products and have shown therapeutic potential (Perez-Vizcaino et al. 2018). Some of them are good candidates for further clinical studies as antibiotics alone or in combination with conventional antibiotics (Amin et al. 2015). The flavonoid icariin (Fig. 1), isolated from the traditional Chinese medicine, *Herba Epimedii*, has shown considerable pharmacological effects (Chen et al. 2011).

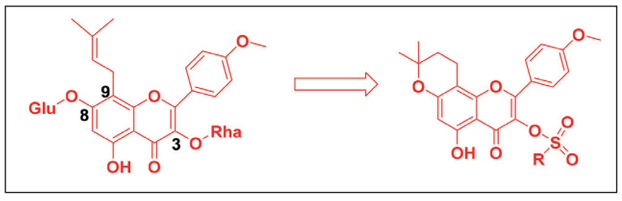

Fig. 1: Icariin and derivatives

In order to achieve potential antibacterial agents, icariin was structurally modified in our study. The design of compounds can be divided into two steps: (i) removing sugar groups and dehydrating –OH at C-8 to form ether with the Pr at C-9 of icariin to improve its fatsoluble; (ii) introducing aromatic sulfonyls at C-3 position, which was expected to increase antibacterial efficacy. All synthesized icariin derivatives were assayed for their antibacterial activity *in vitro* against five *S. aureus* pathogens: MSSA ATCC29213, MRSA ATCC 6538, MRSA ATCC 29213, MRSA ATCC 33591 and MRSA ATCC 43300. Moreover, we studied their antibacterial mechanism based on the most active compound.

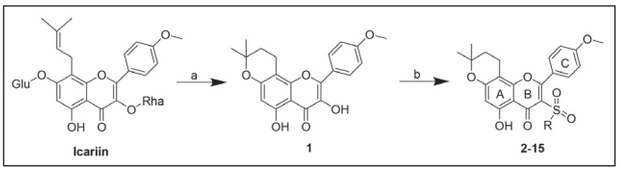

Scheme: Synthesis routes and structure of icariin derivatives. (a) 20% H_2SO_4, MeOH, reflux, 2 h; (g) $ClSO_2R$, Triethylamine, CH_2Cl_2, 25 °C, 4 h.

2. Investigations, results and discussion

2.1. Chemistry

The preparation of icariin derivatives (**2**-**15**) was accomplished using the general method outlined in the Scheme. The key intermediate of compound **1** was obtained from icariin by hydrolysis following a procedure reported earlier (Liu et al. 2009). Then, the substitution reaction of compound **1** with various aromatic sulfonyl chloride gave the target compounds **2**-**15**.

2.2. Antibacterial activity

Antibacterial activity results are listed in Table 1. Most synthesized icariin derivatives showed significant antibacterial activity against the tested microorganisms. A comparison of the results indicated that the existence of the C-3 location had a significant effect. Phenylsulfonyl substituted icariin derivatives **6**, **9** and **10** exhibited 4- to 16-fold more potent antibacterial activity than ciprofloxacin, which were the most active compounds having a MIC value of 1 mmol/L. Thienylsulfonyl substituted icariin derivatives **2**, **3**, **4** and **5** showed *in vitro* activities obviously weaker than ciprofloxacin. Changing the substituents at the backbone of phenyl could remarkably influence the antibacterial activity of these compounds. Electron-withdrawing groups incorporated into the benzyl backbone were better than that electron-donating groups. Electron-withdrawing -F, and $-CF_3$ substituents on *para*-position displayed higher activity than that on *ortho*- and *meta*-positions. Nevertheless, existing research data were insufficient to discuss the structure–function relationship of antibacterial effect of these compounds due to the limited number of synthesized compounds.

Table 1: Antibacterial activities of the target compounds against *S. aureus*

Compd.	R	*S. aureus* MIC (mmol/L)				
		MSSA	MRSA			
		ATCC29213	ATCC6538	ATCC29213	ATCC33591	ATCC43300
2		32	64	32	64	64
3	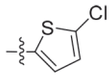	8	16	16	16	16
4	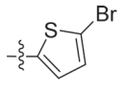	16	32	32	32	16
5	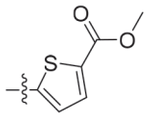	> 128	> 128	> 128	> 128	> 128
6	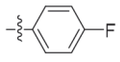	1	2	2	2	1
7		32	16	16	32	16
8	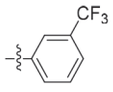	16	32	16	16	32
9	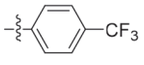	1	1	1	2	2
10	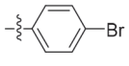	4	16	8	8	16
11	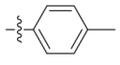	64	128	64	128	> 128
12	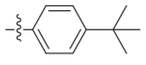	> 128	> 128	> 128	> 128	> 128
13	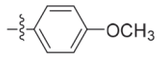	32	16	32	32	32
14	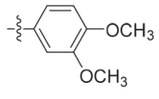	64	64	128	64	128
15	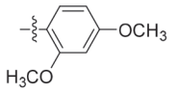	64	128	64	128	64
Ciprofloxacin		4	16	8	8	16

Our future studies may focus on the design and synthesis of additional compounds.

2.3. Preliminary mechanistic studies

2.3.1. Reverse virtual screening

Reverse virtual screening (Ji et al. 2018) was conducted to evaluate the antibacterial mechanism of icariin derivative **9**. The fit value score was employed to evaluate the binding affinity between the ligand with the receptors, and the top 10 disease-related receptors ware shown in Table 2. Among these targets, penicillin-binding protein 2a (PBP2a, PDB 4CJN) was focused, which was a critical target-related bacterial resistance (Mahasenan et al. 2017; Rani et al. 2016). This protein expressed in MRSA strains was the major driver of antimicrobial resistance, for the low affinity for most of *b*-lactam antibiotics.

2.3.2. Molecular docking studies

Molecular docking studies have shown that PBP2a has two binding sites, including an active site and an allosteric site. The earlier struc-

Table 2: Top 10 putative protein targets of title compound 9 predicted by Discovery Studio 2017 R2

Rank	PDB ID	Putative target	Fit value
1	3G4K	Human phosphodiesterase 4d	0.9759
2	2GZ7	SARS-CoV M^{pro}	0.9701
3	2QC6	Protein kinase CK2	0.9446
4	4CJN	Penicillin-binding protein 2a	0.9315
5	3L9H	Mitotic kinesin-5	0.9293
6	1DI8	Cyclin-dependent kinase 2	0.9270
7	3D28	HCV NS5B polymerase	0.9269
8	3C06	Bacterial thymidylate synthase	0.9243
9	2DQ7	human Fyn kinase domain	0.9162
10	4EO6	HCV NS5B polymerase	0.9005

ture determination for PBP2a showed a closed active site conformation. Indeed, many studies have been approved that binding of a ligand to the allosteric site imparts conformational opening of the active site, and predisposes PBP2a to inactivation and thus, allosteric binding sites can be targets for new drugs (Rani et al. 2016; Acebrón et al. 2015). Some non-b-lactam antibiotics have been reported to exhibit *in vitro* and *in vivo* activity against MRSA by binding to the allosteric site of PBP2a (Bouley et al. 2015; Peters et al. 2018; Decuyper et al. 2018). Analysis of the docking results revealed that compound **9** shows a common binding mode into the PBP2a (PDB 4CJN) allosteric binding site with a well steric and electronic complementarity (Fig. 2). There were multiple obvious bonding interactions anchoring compound **9** to the allosteric site tightly might explain its well antibacterial activity. Frist, the C ring of **9** inserted into the allosteric site deeply and had hydrophobic interactions with residues of GLU 294, ASP295. Second, three hydrogen bonds can be found between the substituted aromatic sulfonyl moiety and the receptor (one O atom on sulfonic group with TYR105; two F atoms on trifluoromethyl with LYS316 respectively). Another one hydrogen bond interaction was between the methoxyol on C ring with ASP275. Third, two strong attractive Pi-Pi stacking were formed between the residue of TYR105 with A ring and B ring. Furthermore, two Pi-cation interactions were formed (LYS 273 with C ring; LYS 316 with phenyl of the aromatic sulfonyl moiety).

2.3.3. Surface plasmon resonance (SPR) assay

To confirm the binding affinity of title compound **9** with PBP2a, a surface plasmon resonance (SPR) assay was performed. PBP2a protein was immobilized on the sensor chip, and binding responses in response units (RU) were continuously recorded and graphically presented as a function of time in sensograms. The association of compound **9** with PBP2a was evaluated using the equilibrium dissociation constant (KD) by fitting the sensogram with a 1:1 (Langmuir) binding fit model. As shown in Fig. 3, compound **9** had a high binding affinity toward PBP2a in a concentration-dependent manner. KD value was calculated to be 1.82×10^{-7} M.

In summary, a new set of aromatic sulfonyls substituted icariin derivatives was synthesized from icariin in order to get potential

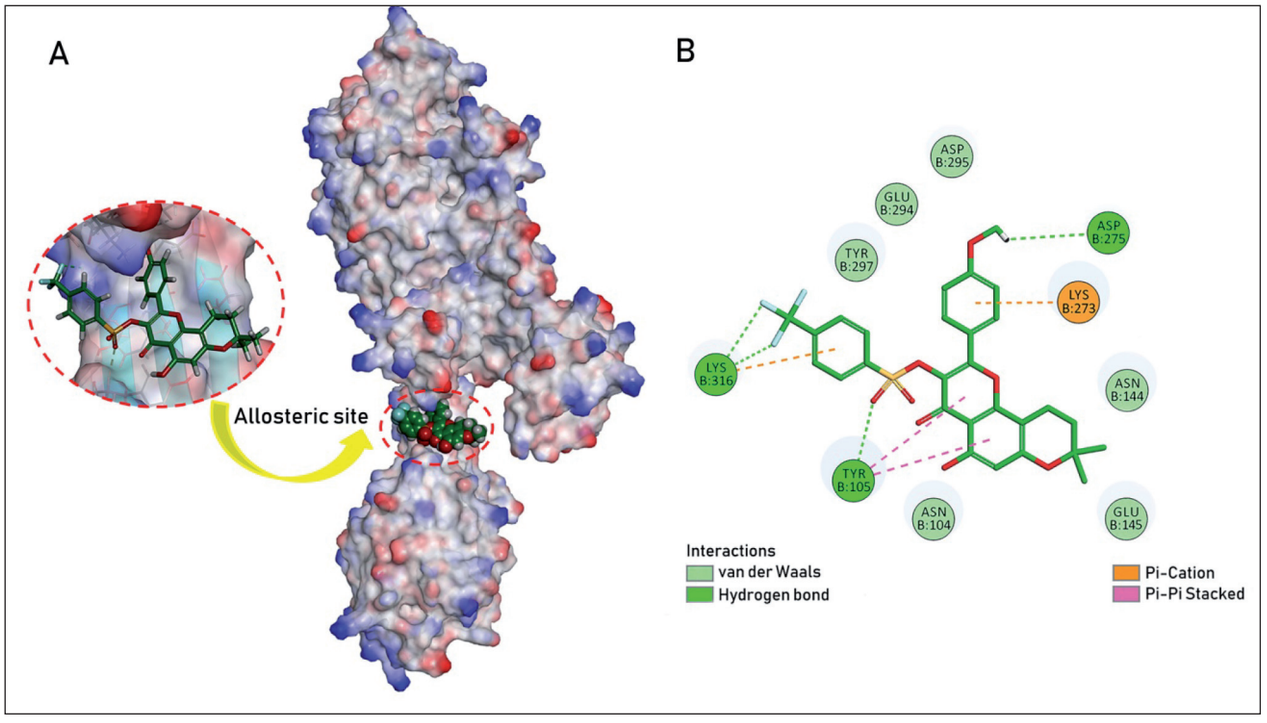

Fig. 2: (A) 3D model of the interaction between compound 9 with PBP2a (PDB 4CJN). (B) 2D binding mode within the receptor PBP2a allosteric site pocket. These Figures were produced using the Discovery Studio 2017 R2 software.

antibacterial agents. Their antibacterial activities were evaluated using five *S. aureus* pathogens: MSSA ATCC29213, MRSA ATCC 6538, MRSA ATCC 29213, MRSA ATCC 33591 and MRSA ATCC 43300. The results showed that most synthesized compounds can resist selected microorganisms to some extent. Among them, compound **9** was the most active compound having a MIC value of 1-2 mmol/L. Reverse virtual screening and molecule docking revealed that compound 9 can bind well with the allosteric site of PBP2a of *S. aureus* through multiple actions. SPR further proved the in vitro binding between **9** and PBP2a. These findings suggesting a starting point for designing more effective compounds against MRSA strains.

3. Experimental

3.1. Synthesis and characterization

NMR spectra were recorded on a Bruker 400 NMR with tetramethylsilane (TMS) as an internal standard. MS spectra were obtained

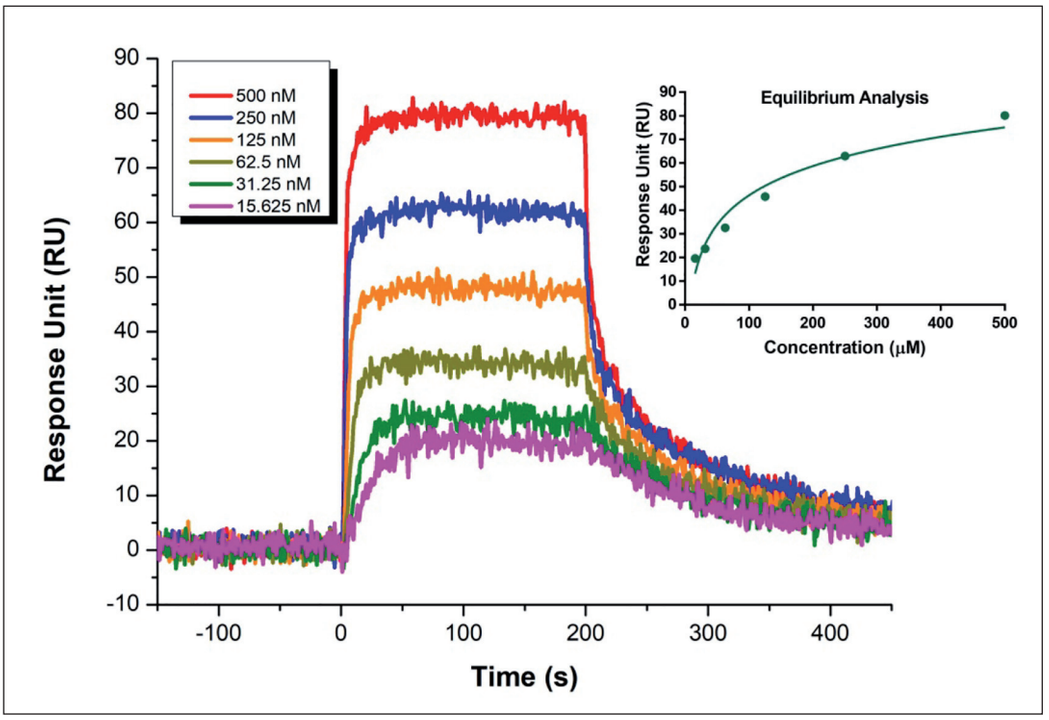

Fig. 3: Surface plasmon resonance (SPR) sensograms for compound **9** binding to the immobilized PBP2a. As shown in the plot, ligand concentrations in the flow solutions were 500, 250, 125, 62.5, 31.25, and 15.625 nM for the curves from bottom to top.

using Shimadzu LC-MS-2010A spectrometry. Melting points were determined on a XT4MP apparatus (Taike Corp., Beijing, China), and are uncorrected. Elemental analysis was measured by the Elementar Vario EL CHNS Elemental Analyzer (Elementar, Hanau, Germany).

*3.1.2. 3,5-Dihydroxy-2-(4-methoxyphenyl)-8,8-dimethyl-9,10-dihydropyrano[2,3-f]chromen-4(8H)-one (**1**)*

Compound **1** was synthesized as reported (Liu et al. 2009). Light yellow solid; yield 2.34 g, 86 %; m.p. 223-225 °C; ^{1}H NMR (400 MHz, DMSO-d_6): δ 12.20 (s, 1H), 9.57 (s, 1H), 8.17 (d, J = 9.0 Hz, 2H), 7.13 (d, J = 9.0 Hz, 2H), 6.14 (s, 1H), 3.85 (s, 3H), 2.85 (t, J = 6.6 Hz, 2H), 1.87 (t, J = 6.6 Hz, 2H), 1.34 (s, 6H); APCI-MS m/z: 367 $[M + H]^+$. Anal. calcd. for $C_{21}H_{20}O_6$. H_2O: C, 65.28; H, 5.74. Found: C, 65.21; H, 5.79.

*3.1.3. Preparation of compounds **2-15***

To a mechanically stirred suspension of suspension of **1** (0.21 g, 0.53 mmol) in 30 ml CH_2Cl_2 were added triethylamine (0.5 ml) and aromatic sulfonyl chloride (0.53 mmol) at 25 °C for 4 h. The reaction process was detected by TLC method. Then, antagonized by dilute sodium hydroxide, extracted, and washed with ether and water, evaporated under vacuum. Finally, the mixture was recrystallized from ethyl acetate , providing a total product yield of 65.4%-88.6 %.

*2-(11-Chlorobenzofuro[3,2-b]quinolin-7-yloxy)-N,N-dimethylethanamine (**2**):* Yellow solid; yield 0.2 g, 77.1 %; m. p. 218-219 °C; ^{1}H NMR (400 MHz, DMSO-d_6): δ 11.85 (s, 1H), 8.05 (d, J = 6.1 Hz, 1H), 7.82 (d, J = 8.9 Hz, 2H), 7.69 (d, J = 5.0 Hz, 1H), 7.09 – 7.04 (m, 1H), 6.99 (d, J = 8.9 Hz, 2H), 6.24 (s, 1H), 3.84 (s, 3H), 2.82 (t, J = 6.7 Hz, 2H), 1.85 (t, J = 6.6 Hz, 2H), 1.34 (s, 6H); APCI-MS m/z: 513 $[M + H]^+$; Anal. calcd. for $C_{25}H_{22}O_8S_2$. $2H_2O$: C, 58.36; H, 4.31. Found: C, 58.37; H, 4.32.

*5-Hydroxy-2-(4-methoxyphenyl)-8,8-dimethyl-4-oxo-4,8,9,10-tetrahydropyrano[2,3-f]chromen-3-yl 5-chlorothiophene-2-sulfonate (**3**)*: Yellow solid; yield 0.13 g, 72.4 %; m. p. 223-224 °C; ^{1}H NMR (400 MHz, DMSO-d_6): δ 7.89 (d, J = 9.0 Hz, 2H), 7.51 (d, J = 4.1 Hz, 1H), 6.98 (d, J = 9.0 Hz, 2H), 6.86 (d, J = 4.1 Hz, 1H), 6.30 (s, 1H), 3.91 (s, 3H), 2.86 (t, J = 6.8 Hz, 2H), 1.89 (t, J = 6.8 Hz, 2H), 1.40 (s, 6H); APCI-MS m/z: 547 $[M + H]^+$; Anal. calcd. for $C_{25}H_{21}ClO_8S_2$. H_2O: C, 52.96; H, 4.09. Found: C, 52.95; H, 4.97.

*5-Hydroxy-2-(4-methoxyphenyl)-8,8-dimethyl-4-oxo-4,8,9,10-tetrahydropyrano[2,3-f]chromen-3-yl 5-bromothiophene-2-sulfonate (**4**)*: Yellow solid; yield 0.19 g, 88.6 %; m. p. 222-224 °C; ^{1}H NMR (400 MHz, DMSO-d_6): δ 11.85 (s, 1H), 7.75 (d, J = 8.9 Hz, 2H), 7.55 (d, J = 4.1 Hz, 1H), 7.18 (d, J = 4.1 Hz, 1H), 6.99 (d, J = 8.9 Hz, 2H), 6.25 (s, 1H), 3.86 (s, 3H), 2.81 (t, J = 6.6 Hz, 2H), 1.85 (t, J = 6.6 Hz, 2H), 1.34 (s, 6H); APCI-MS m/z: 592 $[M + H]^+$; Anal. calcd. for $C_{25}H_{21}BrO_8S_2$. H_2O: C, 49.11; H, 3.79. Found: C, 49.09; H, 3.80.

*Methyl-3-(((5-hydroxy-2-(4-methoxyphenyl)-8,8-dimethyl-4-oxo-4,8,9,10-tetrahydropyrano[2,3-f]chromen-3-yl)oxy) sulfonyl)thiophene-2-carboxylate (**5**)*: Yellow solid; yield 0.14 g, 69 %; m.p. 220-221 °C; ^{1}H NMR (400 MHz, DMSO-d_6): δ 11.81 (s, 1H), 7.87 (d, J = 5.3 Hz, 1H), 7.82 (d, J = 8.9 Hz, 2H), 7.32 (d, J = 5.3 Hz, 1H), 6.97 (d, J = 8.9 Hz, 2H), 6.24 (s, 1H), 3.89 (s, 3H), 3.84 (s, 4H), 2.81 (t, J = 6.6 Hz, 2H), 1.85 (t, J = 6.6 Hz, 2H), 1.34 (s, 6H); APCI-MS m/z: 571 $[M + H]^+$; Anal. calcd. for $C_{27}H_{24}O_{10}S_2$. H_2O: C, 54.91; H, 4.44. Found: C, 54.93; H, 4.43.

*5-Hydroxy-2-(4-methoxyphenyl)-8,8-dimethyl-4-oxo-4,8,9,10-tetrahydropyrano[2,3-f]chromen-3-yl 4-fluorobenzenesulfonate (**6**)*: Yellow solid; yield 0.12 g, 74.8 %; m. p. 218-219 °C; ^{1}H NMR (400 MHz, DMSO-d_6): δ 11.85 (s, 1H), 7.82 (dd, J = 8.9, 5.0 Hz, 2H), 7.73 (d, J = 8.9 Hz, 2H), 7.28 (t, J = 8.8 Hz, 2H), 6.93 (d, J = 8.9 Hz, 2H), 6.24 (s, 1H), 3.83 (s, 3H), 2.80 (t, J = 6.7 Hz, 2H), 1.85 (t, J = 6.7 Hz, 2H), 1.34 (s, 6H); APCI-MS m/z: 525 $[M + H]^+$; Anal. calcd. for $C_{27}H_{23}FO_8S$: C, 61.59; H, 4.40. Found: C, 61.61; H, 4.39.

*5-Hydroxy-2-(4-methoxyphenyl)-8,8-dimethyl-4-oxo-9,10-dihydro-4H,8H-pyrano[2,3-f]chromen-3-yl 2-fluorobenzenesulfonate (**7**)*: Yellow solid; yield 0.12 g, 80.5 %; m. p. 220-222 °C; ^{1}H NMR (400 MHz, $CDCl_3$): δ 8.02 (d, J = 9.0 Hz, 2H), 7.92 (d, J = 7.9 Hz, 1H),

7.69 (t, J = 8.7 Hz, 1H), 7.46 (d, J = 8.3 Hz, 1H), 7.37 (t, J = 7.7 Hz, 1H), 7.00 (d, J = 9.0 Hz, 2H), 6.25 (s, 1H), 3.91 (s, 3H), 2.86 (t, J = 6.8 Hz, 2H), 1.88 (t, J = 6.8 Hz, 2H), 1.39 (s, 6H); APCI-MS m/z: 525 $[M + H]^+$; Anal. Calcd. for $C_{27}H_{23}FO_8S$: C, 61.59; H, 4.40. Found: C, 61.62; H, 4.42.

*5-Hydroxy-2-(4-methoxyphenyl)-8,8-dimethyl-4-oxo-4,8,9,10-tetrahydropyrano[2,3-f]chromen-3-yl 3-(trifluoromethyl)benzenesulfonate (**8**):* Yellow solid; yield 0.124 g, 75.4 %; m p. 217-218 °C; ^{1}H NMR (400 MHz, DMSO-d_6): δ 11.80 (s, 1H), 8.13 (d, J = 8.0 Hz, 1H), 8.06 (d, J = 7.9 Hz, 1H), 7.94 (s, 1H), 7.75 (dd, J = 15.6, 8.4 Hz, 4H), 6.87 (d, J = 8.9 Hz, 1H), 6.25 (s, 1H), 3.80 (s, 3H), 2.80 (t, J = 6.7 Hz, 2H), 1.85 (t, J = 6.6 Hz, 2H), 1.34 (s, 6H); APCI-MS m/z: 575 $[M + H]^+$; Anal. calcd. for $C_{28}H_{23}F_3O_8S$. H_2O: C, 56.56; H, 4.24. Found: C, 56.54; H, 4.27.

*5-Hydroxy-2-(4-methoxyphenyl)-8,8-dimethyl-4-oxo-4,8,9,10-tetrahydropyrano[2,3-f]chromen-3-yl 3,5-difluorobenzenesulfonate (**9**):* Yellow solid; yield 0.135 g, 65.4 %; m. p. 226-227 °C; ^{1}H NMR (400 MHz, DMSO-d6): δ 11.81 (s, 1H), 7.94 (s, 2H), 7.78 (d, J = 8.4 Hz, 2H), 7.68 (d, J = 8.9 Hz, 2H), 6.85 (s, 2H), 6.25 (s, 1H), 3.79 (s, 3H), 2.79 (t, J = 6.7 Hz, 2H), 1.84 (t, J = 6.6 Hz, 2H), 1.34 (s, 6H); APCI-MS m/z: 575 $[M + H]^+$; Anal. calcd. for $C_{28}H_{23}F_3O_8S$: C, 58.33; H, 4.02. Found: C, 58.30; H, 3.99.

*5-Hydroxy-2-(4-methoxyphenyl)-8,8-dimethyl-4-oxo-4,8,9,10-tetrahydropyrano[2,3-f]chromen-3-yl 4-bromobenzenesulfonate (**10**)***:*** Yellow solid; yield 0.27 g, 70.4 %; m. p. 224-225 °C; ^{1}H NMR (400 MHz, DMSO-d_6): δ 11.76 (s, 1H), 8.20 (d, J = 8.8 Hz, 2H), 8.00 (d, J = 8.8 Hz, 2H), 7.67 (d, J = 8.9 Hz, 2H), 6.86 (d, J = 8.9 Hz, 2H), 6.24 (s, 1H), 3.77 (s, 3H), 2.79 (t, J = 6.6 Hz, 2H), 1.84 (t, J = 6.6 Hz, 2H), 1.34 (s, 6H); APCI-MS m/z: 585 $[M + H]^+$; Anal. calcd. for $C_{27}H_{23}BrO_8S$: C, 55.21; H, 3.95. Found: C, 55.19; H, 3.96.

*5-Hydroxy-2-(4-methoxyphenyl)-8,8-dimethyl-4-oxo-4,8,9,10-tetrahydropyrano[2,3-f]chromen-3-yl 4-methylbenzenesulfonate (**11**)*: Yellow solid; yield 0.178 g, 78.6 %; m. p. 219-221 °C; ^{1}H NMR (400 MHz, DMSO-d_6): δ 11.91 (s, 1H), 7.70 (d, J = 8.8 Hz, 2H), 7.59 (d, J = 8.2 Hz, 2H), 7.23 (d, J = 8.1 Hz, 2H), 6.90 (d, J = 8.9 Hz, 2H), 6.24 (s, 1H), 3.83 (s, 3H), 2.80 (t, J = 6.6 Hz, 2H), 1.84 (t, J = 6.6 Hz, 2H), 1.34 (s, 6H), 1.24 (s, 3H); APCI-MS m/z: 521 $[M + H]^+$; APCI-MS m/z: 521 $[M + H]^+$; Anal. calcd. for $C_{28}H_{26}O_8S$. H_2O: C, 62.21; H, 5.22. Found: C, 62.23; H, 5.24.

*5-Hydroxy-2-(4-methoxyphenyl)-8,8-dimethyl-4-oxo-9,10-dihydro-4H,8H-pyrano[2,3-f]chromen-3-yl 4-(tert-butyl)benzenesulfonate (**12**)*: Yellow solid; yield 0.18 g, 72.9 %; m. p. 223-224 °C; ^{1}H NMR (400 MHz, DMSO-d_6): δ 11.91 (s, 1H), 7.71 (d, J = 8.9 Hz, 2H), 7.64 (d, J = 8.6 Hz, 2H), 7.43 (d, J = 8.6 Hz, 2H), 6.88 (d, J = 8.9 Hz, 2H), 6.24 (s, 1H), 3.81 (s, 3H), 2.80 (t, J = 6.6 Hz, 2H), 1.85 (t, J = 6.6 Hz, 2H), 1.34 (s, 6H), 1.26 (s, 9H); APCI-MS m/z: 563 $[M + H]^+$; APCI-MS m/z: 563 $[M + H]^+$; Anal. calcd. for $C_{31}H_{32}O_8S$. H_2O: C, 63.90; H, 5.88. Found: C, 63.88; H, 5.91.

*5-Hydroxy-2-(4-methoxyphenyl)-8,8-dimethyl-4-oxo-4,8,9,10-tetrahydropyrano[2,3-f]chromen-3-yl 4-methoxybenzenesulfonate (**13**)***:*** Yellow solid; yield 0.18 g, 82.8 %; m. p. 213-215 °C; ^{1}H NMR (400 MHz, DMSO-d_6): δ 11.94 (s, 1H), 7.71 (d, J = 8.9 Hz, 2H), 7.63 (d, J = 8.9 Hz, 2H), 6.91 (dd, J = 9.0, 2.1 Hz, 4H), 6.23 (s, 1H), 3.82 (s, 6H), 2.80 (t, J = 6.7 Hz, 2H), 1.85 (t, J = 6.6 Hz, 2H), 1.34 (s, 6H); APCI-MS m/z: 537 $[M + H]^+$; Anal. calcd. for $C_{28}H_{26}O_9S$: C, 62.44; H, 4.87. Found: C, 62.41; H,4.86.

*5-Hydroxy-2-(4-methoxyphenyl)-8,8-dimethyl-4-oxo-4,8,9,10-tetrahydropyrano[2,3-f]chromen-3-yl 3,4-dimethoxybenzenesulfonate (**14**)* Yellow solid; yield 0.122 g, 65.4 %; m. p. 216-217 °C; ^{1}H NMR (400 MHz, DMSO-d_6): δ 11.99 (s, 1H), 7.64 (d, J = 8.9 Hz, 2H), 7.29 (d, J = 10.7 Hz, 1H), 7.01 (s, 1H), 6.91 (d, J = 8.6 Hz, 1H), 6.83 (d, J = 8.9 Hz, 2H), 6.24 (s, 1H), 3.81 (d, J = 13.5 Hz, 6H), 3.70 (s, 3H), 2.79 (t, J = 6.6 Hz, 2H), 1.84 (t, J = 6.6 Hz, 2H), 1.34 (s, 6H); APCI-MS m/z: 567 $[M + H]^+$; Anal. calcd. for $C_{29}H_{28}O_{10}S$. H_2O: C, 59.38; H, 5.16. Found: C, 59.37; H, 5.19.

*5-Hydroxy-2-(4-methoxyphenyl)-8,8-dimethyl-4-oxo-4,8,9,10-tetrahydropyrano[2,3-f]chromen-3-yl 2,4-dimethoxybenzenesulfonate (**15**)*: Yellow solid; yield 0.155 g, 72.6 %; m. p. 213-215 °C; ^{1}H NMR (400 MHz, DMSO-d_6): δ 11.95 (s, 1H), 7.73 (d, J = 8.9 Hz, 2H), 7.40 (d, J = 8.9 Hz, 1H), 6.92 (d, J = 8.9 Hz, 2H), 6.53 (s, 1H), 6.44 (d, J = 8.9 Hz, 1H), 6.22 (s, 1H), 3.82 (s, 9H), 2.79 (t, J = 6.6 Hz, 2H), 1.84 (t, J = 6.6 Hz, 2H), 1.33 (s, 6H); APCI-MS m/z: 567 $[M + H]^+$; Anal. calcd. for $C_{29}H_{28}O_{10}S$. $2H_2O$: C, 57.61; H, 5.33. Found: C, 57.58; H, 5.37.

3.2. Determination of MIC

The MIC of the synthesized compounds was determined for each of the tested organisms in triplicates. Varying concentrations of the samples (128.0, 64.0, 32.0, 16.0, 8.0, 4.0, 2.0, 1.0 and 0.5 mmol/L), nutrient broth were added and then a loopful of the test organism previously diluted to 0.5 McFarland turbidity standard was introduced to the tubes. Levofloxacin was used as positive controls. Then tubes containing tested organisms cultures were then incubated at 37 °C for 24 h. The tubes were then examined for growth by observing for turbidity. All microorganism was supplied by the Department of Clinical Laboratory, First Affiliated Hospital of Anhui Medical University.

3.3. Reverse virtual screening and molecule docking

Reverse virtual screening was performed using Discovery Studio 2017 R2 soft. The ligand structure was drawn and optimized by using DS 2017 R2. The initial three dimensional geometric coordinates of the X-ray crystal structure of macromolecule targets were obtained from the Protein Databank (PDB) by using DS 2017 R2. The LibDock protocol were employed as reverse virtual screening to conduct semi-flexible docking. The X-ray structure of MetAP1 (PDB: 4npc) was also obtained from Protein Databank (PDB). Before going to the docking procedure, the protein structure was prepared using the Protein preparation wizard of the DS 2017 R2. CDocker protocol was used for the molecule docking.

3.4. SPR experiment

A SPR experiment was performed at 25 °C with a Biacore T200 apparatus on CM5 sensor chips (GE Healthcare, Fairfield, CT, USA). CM5 sensor chip was activated, and PBP2a protein in 10 mM NaAc (pH 5.5) was immobilized at densities of approximately 400 RUs. The samples were prepared in PBS with Tween 20 (PBS-T) (137 mM NaCl, 2.7 mM KCl, 1.5 mM KH2PO4, 8.1 mM Na2HPO4, 0.05% Tween 20, pH 7.35) running buffer and were injected over the functionalized surface at a flow rate of 30 µL/min for an association phase of 120 s and a dissociation phase of 90 s. After each injection, the sensor chip surface was completely regenerated with PBS (pH 7.4) at a flow rate of 10 µL/min for 60 s. Running buffer (blank control) was made to flow over the chip, and sensorgrams were obtained after blank subtraction. The sensorgrams were analyzed with the Biacore T200 evaluation software (version 2.0, Fairfield, CT, USA). The kinetic parameters, including association rate constants (ka), dissociation rate constants (kd), and kinetic dissociation constant (KD), were calculated by Biacore T200 evaluation software 2.1 (Fairfield, CT, USA).

Acknowledgments: This work was supported by the Key University Science Research Project of Anhui Province (KJ2018A0210). Y. X. designed the work. A. W. contributed to the synthesis and of the compound. A. W. and L. Z. evaluation of the biological activity.

Conflicts of interest: None declared.

References

Acebrón I, Chang M, Mobashery S, Hermoso JA (2015) The allosteric site for the nascent cell wall in penicillin-binding protein 2a: an Achilles' heel of methicillin-resistant Staphylococcus aureus. Curr Med Chem 22: 1678-1686.

Amin MU, Khurram M, Khattak B, Khan J (2015) Antibiotic additive and synergistic action of rutin, morin and quercetin against methicillin resistant Staphylococc us aureus. BMC Complem Altern Med 15: 59.

Bouley R, Kumarasiri M, Peng Z, Otero LH, Song W, Suckow MA, Schroeder VA, Wolter WR, Lastochkin E, Antunes NT, Pi H, Vakulenko S, Hermoso JA, Chang M, Mobashery S (2015) Discovery of antibiotic (E)-3-(3-carboxyphenyl)-2-(4-cyanostyryl)quinazolin-4(3H)-one. J Am Chem Soc 137: 1738-1741.

Chen Y, Huang JH, Ning Y, Shen ZY (2011) Icariin and its pharmaceutical efficacy: research progress of molecular mechanism. Zhong Xi Yi Jie He Xue Bao 9: 1179-1184.

Decuyper L, Deketelaere S, Vanparys L, Jukič M, Sosič I, Sauvage E, Amoroso AM, Verlaine O, Joris B, Gobec S, D'hooghe M (2018) In silico design and enantioselective synthesis of functionalized monocyclic 3-amino-1-carboxymethyl-β-lactams as inhibitors of penicillin-binding proteins of resistant bacteria. Chemistry 24: 15254-15266.

Lazaris A, Coleman DC, Kearns AM, Pichon B, Kinnevey PM, Earls MR, Boyle B, O'Connell B, Brennan GI, Shore AC (2017) Novel multiresistance cfr plasmids in linezolid-resistant methicillin-resistant Staphylococcus epidermidis and vancomycin-resistant Enterococcus faecium (VRE) from a hospital outbreak: co-location of cfr and optrA in VRE. J Antimicrob Chemother 72: 3252-3257.

Liu DF, Li YP, Ou TM, Huang SL, Gu LQ, Huang M, Huang ZS (2009) Synthesis and antimultidrug resistance evaluation of icariin and its derivatives. Bioorg Med Chem Lett 19: 4237-4240.

Ji L, Wu M, Li Z (2018) Rutacecarpine inhibits angiogenesis by targeting the VEGFR2 and VEGFR2-mediated Akt/mTOR/p70s6k signaling pathway. Molecules 23: pii: E2047.

MacAllister TJ, Stohs E, Liu C, Bryan A, Whimbey E, Phipps A, Pergam SA (2018) 10-year trends in vancomycin-resistant enterococci among allogeneic hematopoietic cell transplant recipients. J Infect 77: 38-46.

Mahasenan K, Molina R, Bouley R, Batuecas M, Fisher J, Hermoso JA, Chang M, Mobashery S (2017) Conformational dynamics in penicillin-binding protein 2a of methicillin-resistant Staphylococcus aureus, allosteric communication network and enablement of catalysis. J Am Chem Soc 139: 2102-2110.

Mamishi S, Moradkhani S, Mahmoudi S, Hosseinpour-Sadeghi R, Pourakbari B (2014) Penicillin-Resistant trend of Streptococcus pneumoniae in Asia: A systematic review. Iran J Microbiol 6: 198-210.

Parrish KL, Hogan PG, Clemons AA, Fritz SA (2018) Spatial relationships among public places frequented by families plagued by methicillin-resistant Staphylococcus aureus. BMC Res Notes 11: 692.

Perez-Vizcaino F, Fraga CG (2018) Research trends in flavonoids and health. Arch Biochem Biophys 646: 107-112.

Peters K, Pazos M, Edoo Z, Hugonnet JE, Martorana AM, Polissi A, VanNieuwenhze MS, Arthur M, Vollmer W (2018) Copper inhibits peptidoglycan LD-transpeptidases suppressing β-lactam resistance due to bypass of penicillin-binding proteins. Proc Natl Acad Sci USA. 2018, 115, 10786-10791.

Rani N, Vijayakumar S, Lakshmi PTV, Arunachalam A (2016) Allosteric site-mediated active site inhibition of PBP2a using Quercetin 3-O-rutinoside and its combination. J Biomol Struct Dyn 34: 1778-1796.